EPA-600/4-76-021
May 1976

Environmental Monitoring Series

# A NUMERICAL AND EXPERIMENTAL STUDY OF STABLY STRATIFIED FLOW AROUND COMPLEX TERRAIN


Environmental Sciences Research Laboratory
Office of Research and Development
U.S. Environmental Protection Agency
Research Triangle Park, North Carolina 27711

## RESEARCH REPORTING SERIES

Research reports of the Office of Research and Development, U.S. Environmental Protection Agency, have been grouped into five series. These five broad categories were established to facilitate further development and application of environmental technology. Elimination of traditional grouping was consciously planned to foster technology transfer and a maximum interface in related fields. The five series are:

1. Environmental Health Effects Research
2. Environmental Protection Technology
3. Ecological Research
4. Environmental Monitoring
5. Socioeconomic Environmental Studies

This report has been assigned to the ENVIRONMENTAL MONITORING series. This series describes research conducted to develop new or improved methods and instrumentation for the identification and quantification of environmental pollutants at the lowest conceivably significant concentrations. It also includes studies to determine the ambient concentrations of pollutants in the environment and/or the variance of pollutants as a function of time or meteorological factors.

This document is available to the public through the National Technical Information Service, Springfield, Virginia 22161.

EPA-600/4-76-021
May 1976

# A NUMERICAL AND EXPERIMENTAL STUDY OF STABLY STRATIFIED FLOW AROUND COMPLEX TERRAIN

by

J. J. Riley, H. T. Liu and E. W. Geller
Flow Research, Inc.
Kent, Washington 98031

Contract No. 68-02-1293

Project Officer

William H. Snyder
Meteorology and Assessment Division
Environmental Sciences Research Laboratory
Research Triangle Park, N.C. 27711

U. S. ENVIRONMENTAL PROTECTION AGENCY
OFFICE OF RESEARCH AND DEVELOPMENT
ENVIRONMENTAL SCIENCES RESEARCH LABORATORY
RESEARCH TRIANGLE PARK, N.C. 27711

## DISCLAIMER

This report has been reviewed by the Environmental Sciences Research Laboratory, U. S. Environmental Protection Agency, and approved for publication. Approval does not signify that the contents necessarily reflect the views and policies of the U. S. Environmental Protection Agency, nor does mention of trade names of commercial products constitute endorsement or recommendation for use.

## PREFACE

Assessment of the environmental impact of releasing pollutants into the atmosphere involves understanding, modeling, and predicting the pollutant diffusion patterns. Prediction is particularly difficult when the pollutants are released into regions of complex terrain features, especially when the ambient atmosphere is stably stratified. Such conditions are also most conducive to severe pollution episodes.

In the past Flow Research has been under contract with the Environmental Protection Agency to conduct laboratory investigations of plume dispersion in stably stratified flows over complex terrain. Under the present contract (No. 68-02-1293) further laboratory studies have been conducted. The results are presented in a final report entitled, "Plume Dispersion in Stably Stratified Flows Over Complex Terrain: Phase 2." Also under this contract, we have developed a computer model to predict plume dispersion around complex terrain for the case of strong stratification and have performed experiments to make preliminary validation of this model. The results of the latter work are presented in this report.

ABSTRACT

A computer program has been developed, based on an expansion suggested by Drazin (1961) and Lilly (1973), to compute three-dimensional stratified flow around complex terrain for the case of very strong stratification (small internal Froude number). Also, laboratory experiments were performed for strongly stratified flow past three different terrain models. Preliminary comparisons of the results of the computer program and the laboratory modeling indicate that the computed results are in fair agreement with the experiments. Discrepancies are probably attributable mainly to the separated wake in the lee of the models. Other possible sources of error are discussed in some detail.

CONTENTS

LIST OF FIGURES

LIST OF TABLES

LIST OF SYMBOLS

| Symbol | Description |
|---|---|
| $D$ | diameter of circular cylinder |
| $\frac{d\bar{\rho}_c}{dx_3}$ | characteristic scale of the ambient density gradient |
| $F$ | $= \frac{U}{Nh}$ , internal Froude number |
| $F_h$ | $= \frac{2\pi U}{Nh}$ , internal Froude number based on the Brunt-Vaisala frequency in cycles/sec. |
| $g$ | acceleration due to gravity |
| $H$ | subscript denoting the horizontal component of a vector |
| $h$ | characteristic vertical scale of the model |
| $L$ | characteristic horizontal scale of the model |
| $N$ | $= \sqrt{-\frac{g}{\rho_o}\frac{d\bar{\rho}_c}{dx_3}}$ , characteristic Brunt-Vaisala frequency, rad./sec. |
| $n$ | vortex shedding frequency, rad./sec. |
| $p$ | nondimensional pressure perturbation from the ambient |
| $\hat{p}$ | dimensional pressure perturbation from the ambient |
| $p^{(n)}$ | $n^{th}$ order expansion variable for $p$ |
| $R$ | $= \frac{UD}{\nu}$ , Reynolds number based on the body diameter |
| $S$ | $= \frac{nU}{D}$ , Strouhal number |
| $U$ | free-stream horizontal wind speed |
| $\underset{\sim}{u}$ | $= (u_1, u_2, u_3)$, nondimensional velocity vector |
| $\hat{\underset{\sim}{u}}$ | $= (\hat{u}_1, \hat{u}_2, \hat{u}_3)$, dimensional velocity vector |
| $\underset{\sim}{u}^{(n)}$ | $= (u_1^{(n)}, u_2^{(n)}, u_3^{(n)})$, $n^{th}$ order expansion variable for $\underset{\sim}{u}$ |

$\underset{\sim}{x}$ = $(x_1, x_2, x_3)$, nondimensional coordinate vector

$\hat{\underset{\sim}{x}}$ = $(\hat{x}_1, \hat{x}_2, \hat{x}_3)$, dimensional coordinate vector

$\nabla$ nondimensional gradient operator

$\hat{\nabla}$ dimensional gradient operator

$\varepsilon$ = $F^2$, expansion parameter

$\nu$ kinematic viscosity

$\rho$ nondimensional density perturbation from the ambient

$\bar{\rho}$ nondimensional ambient density

$\hat{\rho}$ dimensional density perturbation from the ambient

$\hat{\bar{\rho}}$ dimensional ambient density

$\rho^{(n)}$ $n^{th}$ order expansion variable for $\rho$

$\rho_o$ constant characteristic density scale

$\psi$ nondimensional vertical displacement

$\hat{\psi}$ dimensional vertical displacement

$\psi^{(n)}$ $n^{th}$ order expansion variable for $\psi$

# SECTION I

# INTRODUCTION

Assessment of the environmental impact of the release of pollutants into the atmosphere involves the estimation of diffusion patterns under atmospheric conditions ranging from average to extreme. A detailed knowledge of the wind field is important in the estimation of diffusion patterns, especially if the region of release is characterized by complex terrain. Thus, in the assessment of pollution effects, the understanding and prediction of local wind fields is often very important.

One approach to understanding and predicting local wind fields is numerical simulation. However, the numerical simulation of three-dimensional stratified flow over complex terrain is a very difficult task. This difficulty is a result of numerical complications associated with stratification effects and complex boundaries, and also of the limitations imposed by the core size and cycle time of present day computers. Thus, exploration of certain limiting conditions under which the physical, mathematical and numerical problems can be simplified is useful. One such limit is that of very large internal Froude number, i.e., weak stratification, where the tools of three-dimensional potential-flow theory are often available. Another limit is very small internal Froude number, or strong stratification.

When fluid is strongly stably stratified, vertical motions are heavily constrained and fluid elements tend to remain in their horizontal planes. The degree to which they do remain is measured by the ratio of their initial kinetic energy, $\frac{1}{2}\rho_o U^2$ , to the potential energy required to lift the fluid element over or around the obstacle,

$$-\frac{1}{2} g \frac{d\bar{\rho}_c}{dx_3} h^2 .$$

Here, h is the characteristic vertical scale of the obstacle, g is the acceleration due to gravity, and $\frac{d\bar{\rho}_c}{dx_3}$ is a characteristic ambient stratification. The ratio is

$$-\frac{\rho_o U^2}{g \frac{d\bar{\rho}_c}{dx_3} h^2} = \left(\frac{U}{Nh}\right)^2 = F^2 ,$$

the square of the internal Froude number, where

$$N = \sqrt{-\frac{g}{\rho_o}\frac{d\bar{\rho}_c}{dx_3}}$$

is a characteristic Brunt-Vaisala frequency of the ambient fluid. For strongly stratified flows ($F \to 0$), Drazin (1961) and, later, Lilly (1973) have proposed a formal expansion in $F^2$, which predicts that, to the lowest order, the flow resembles two-dimensional (horizontal) flow around contours of terrain at a given level. The deviations from this two-dimensional flow can be determined from the higher order terms in a power series.

In the work discussed in this report, we have developed computer programs to solve the equations resulting from the expansion suggested by Drazin and Lilly. We have also performed laboratory studies of stratified flows past simple terrain configurations to validate the numerical programs. Finally, we have made preliminary comparisons of theory and experiment.

## SECTION II

## SUMMARY, CONCLUSIONS AND RECOMMENDATIONS

We have developed a computer program to predict three-dimensional stably stratified flow around complex terrain. The method is based on scaling analysis suggested by Drazin (1961) and Lilly (1973), and is valid for the case of very strong stratification (small internal Froude number). In order to validate the computer model, we have also conducted laboratory studies of flow past isolated terrain features. Three different terrain models were used, and simulations were performed at several Froude numbers for each model. Then those streamline locations measured in the experiments were compared to those predicted by the computer model.

This study was intended to be a very preliminary examination of the use of the scaling suggested by Drazin and Lilly for the case of very low-Froude-number, three-dimensional flow over complex terrain. Preliminary results indicate the following:

(i) For the Froude number regime studied, the basic scaling suggested was appropriate, and the flow did resemble two-dimensional flow around contours of the terrain model at the appropriate level.

(ii) To improve the numerical model, the inclusion of at least two effects is of primary importance. They are: (a) the displacement effect of the boundary layer, and, more importantly, (b) the displacement effect of the separated wake.

(iii) The prediction of vertical displacement was roughly valid for the case computed, considering that the effects discussed in (ii) were not modeled.

(iv) The accuracy of the lowest order solution depends strongly on the type of terrain feature considered, as well as the vertical level, the lateral distance from the terrain feature, and, of course, the Froude number. For a given Froude number, the agreement between the numerical model and experiment was much better for the idealized complex peak than for the Gaussian and conical models.

(v) The computed vertical displacement can be used to estimate regions of applicability of the lowest order solution.

(vi) Slight unsteadiness in the oncoming flow may be a result of turbulent vortex shedding in the lee of the models.

One obvious improvement can be made in the numerical model. The separated wake can be crudely modeled by standard techniques used in aerodynamics to compute flow past two-dimensional bodies. (Note, however, that one may have to take into account the three-dimensional nature of the boundary layer.)

Several other improvements are also possible. First, one could include the vertical and horizontal shearing of the free-stream flow. Second, the atmospheric boundary layer could be modeled. This modeling can be accomplished most simply by using the computed inviscid flow to drive a turbulent boundary layer model. A more sophisticated approach would allow the computed boundary layer to react back on the inviscid flow. Third, the scaling analysis could include the effect of atmospheric compressibility, although this effect shouldn't be too important because the vertical motions are weak. Fourth, Coriolis forces could be included. Fifth, as discussed by Drazin and Lilly, the scaling breaks down near the model peaks (because the local scale height is very small, and, therefore, the local Froude number is very large). An investigation of the coupling of the present numerical model with some other model near the mountain peaks could be performed. Sixth, turbulent diffusion could be modeled in the plume dispersion process with the turbulent diffusivity related to the local Richardson number. Finally, it is implicit in the scaling analysis that $\frac{d\bar{\rho}_c}{dx_3}$ characterize the complete density profile. For example, in regions where $\frac{d\hat{\bar{\rho}}}{d\hat{x}_3}$ is very small compared to $\frac{d\bar{\rho}_c}{dx_3}$, the expansion will probably break down. So the case of a two-layer fluid (each layer having a different constant density) cannot be treated with the present scaling. Thus, rescaling the equations to include these more general cases would be useful.

## SECTION III

## BRIEF DESCRIPTION OF THEORY

Consider the steady-state flow past a three-dimensional terrain feature with a typical vertical scale, h, and horizontal scale, L, (see figure 1, where the coordinate system is also defined). We assume the oncoming (free-stream) flow has characteristic velocity, U, and characteristic stratification, $d\bar{\rho}_c/dx_3$, which is a constant. We will also make the Boussinesq approximation and will neglect viscous (turbulent) effects. The equations of motion are (see Phillips, 1966):

$$\hat{\underset{\sim}{u}} \cdot \hat{\nabla}\hat{\underset{\sim}{u}} = -\frac{1}{\rho_o}\hat{\nabla}\hat{p} + \frac{\hat{\rho}}{\rho_o}\underset{\sim}{g} \qquad \underset{\sim}{g} = (0,0,-g) \tag{3.1}$$

$$\hat{\nabla} \cdot \hat{\underset{\sim}{u}} = 0 \tag{3.2}$$

and

$$\hat{\underset{\sim}{u}} \cdot \hat{\nabla}\rho + \hat{u}_3 \frac{d\hat{\bar{\rho}}}{d\hat{x}_3} = 0 \ . \tag{3.3}$$

Here, $\hat{\underset{\sim}{u}}$ is the velocity vector, $\hat{\rho}$ is the density fluctuation about the ambient $\hat{\bar{\rho}}$, and $\hat{p}$ is the pressure perturbation about the ambient. The vertical displacement of a fluid element, $\hat{\psi}$, is given by

$$\hat{\underset{\sim}{u}} \cdot \hat{\nabla}\hat{\psi} = \hat{u}_3 \ . \tag{3.4}$$

Following Lilly (1973), we scale the variables as follows:

$$\underset{\sim}{u}_H = \frac{\hat{\underset{\sim}{u}}_H}{U} \ , \tag{3.5a}$$

$$\underset{\sim}{x}_H = \frac{\hat{\underset{\sim}{x}}_H}{L} \ , \tag{3.5b}$$

$$x_3 = \frac{\hat{x}_3}{h} \ , \tag{3.5c}$$

and

$$p = \frac{\hat{p}}{\rho_o U^2} \ , \tag{3.5d}$$

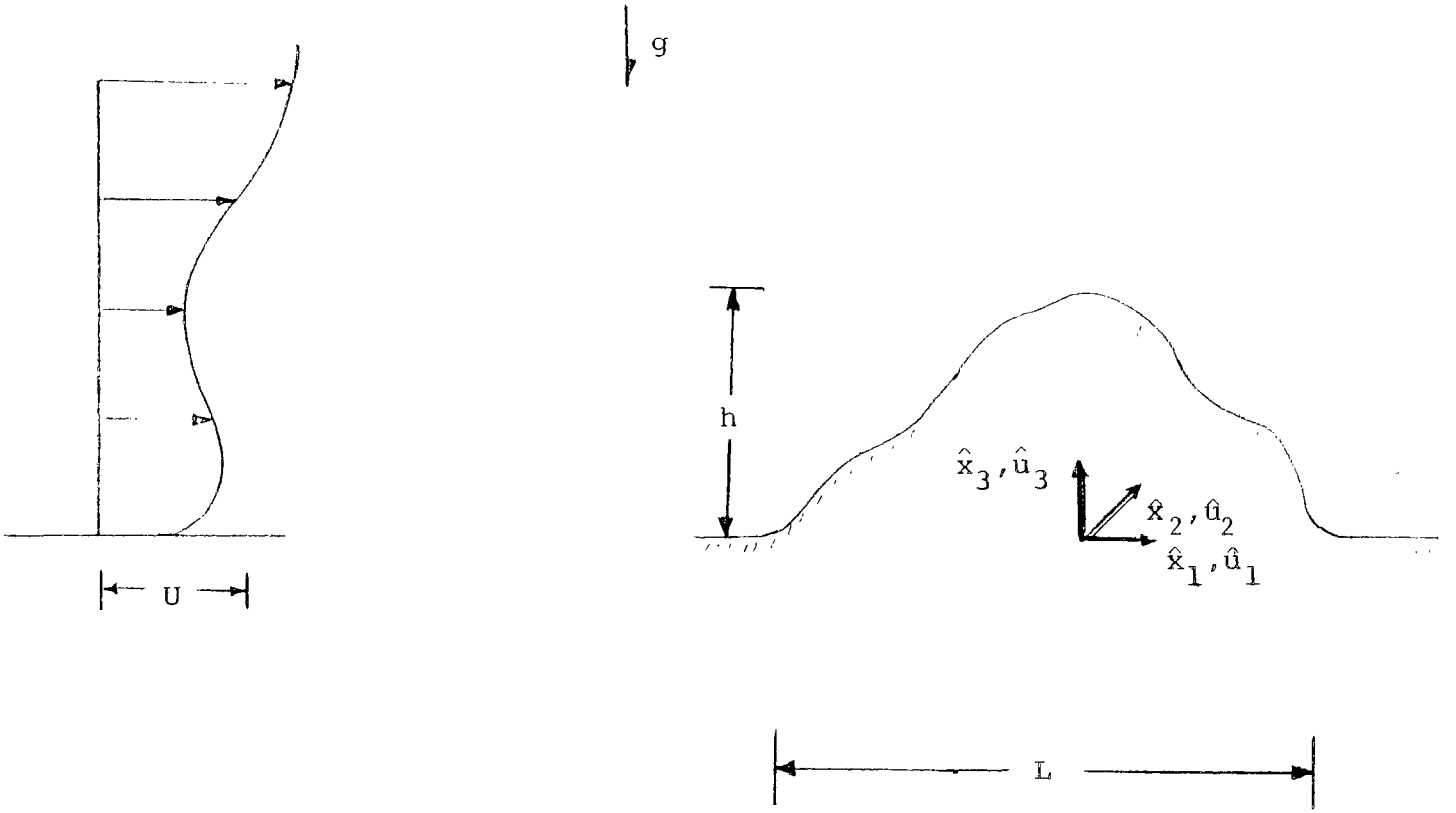


Figure 1. Problem Geometry.

where the subscript, H, denotes the horizontal component of a vector. To scale $\rho$, we assume that $\frac{1}{\rho_o}\frac{\partial \hat{p}}{\partial \hat{x}_3}$ and $\frac{\hat{\rho}}{\rho_o} g$ are in approximate (hydrostatic) balance in the vertical momentum equation. Then,

$$\rho = \frac{\hat{\rho}}{\left(\rho_o U^2\right)/\left(gh\right)} \tag{3.5e}$$

To scale $\hat{u}_3$, we assume that $\hat{u}_3 \frac{d\hat{\bar{\rho}}}{d\hat{x}_3}$ and either $\hat{u}_1 \frac{\partial \hat{\rho}}{\partial \hat{x}_1}$ or $\hat{u}_2 \frac{\partial \hat{\rho}}{\partial \hat{x}_2}$ (or both) are in approximate balance in equation (3.3), which results in

$$u_3 = \frac{\hat{u}_3}{U \frac{h}{L} F^2} , \tag{3.5f}$$

where

$$F = \frac{U}{Nh} \tag{3.6a}$$

is the Froude number,

$$N = \sqrt{-\frac{g}{\rho_o}\frac{d\bar{\rho}_c}{dx_3}} \tag{3.6b}$$

is the characteristic Brunt-Vaisala frequency, and where we scale the ambient stratification (assumed horizontally uniform) as

$$\frac{d\bar{\rho}}{dx_3} = \frac{d\hat{\bar{\rho}}}{d\hat{x}_3} \Big/ \frac{d\bar{\rho}_c}{dx_3} . \tag{3.6c}$$

From (3.4), the scaling for $\hat{\psi}$ is

$$\psi = \frac{\hat{\psi}}{hF^2} . \tag{3.5d}$$

Substituting (3.5) into the horizontal component of (3.1), we find

$$\underset{\sim}{u}_H \cdot \nabla \underset{\sim}{u}_H + F^2 \, u_3 \frac{\partial}{\partial x_3} \underset{\sim}{u}_H = - \nabla_H p \ . \tag{3.7}$$

The vertical component of (3.1) becomes

$$\left(\frac{h}{L}\right)^2 F^2 \, \underset{\sim}{u}_H \cdot \nabla u_3 + \left(\frac{h}{L}\right) F^4 \, u_3 \frac{\partial}{\partial x_3} u_3 = - \frac{\partial p}{\partial x_3} - \rho \ . \tag{3.8}$$

Continuity is now expressed as

$$\nabla \cdot \underset{\sim}{u}_H + F^2 \frac{\partial u_3}{\partial x_3} = 0 \ , \tag{3.9}$$

and the incompressibility condition is

$$\underset{\sim}{u}_H \cdot \nabla \rho + F^2 \, u_3 \frac{\partial \rho}{\partial x_3} - u_3 \frac{d\bar{\rho}}{dx_3} = 0 \ . \tag{3.10}$$

Finally, the equation for $\psi$, the displacement, becomes

$$\underset{\sim}{u}_H \cdot \nabla \psi + F^2 \, u_3 \frac{\partial \psi}{\partial x_3} = u_3 \ . \tag{3.11}$$

Next, we expand the independent variables in the powers of the small parameter, $\varepsilon = F^2$, i.e.,

$$(\underset{\sim}{u}_H, u_3, p, \rho, \psi) = \sum_{n=0}^{\infty} \varepsilon^n \left( \underset{\sim}{u}_H^{(n)}, u_3^{(n)}, p^{(n)}, \rho^{(n)}, \psi^{(n)} \right) . \tag{3.12}$$

The resulting equations to the lowest order are

$$\underset{\sim}{u}_H^{(o)} \cdot \nabla \underset{\sim}{u}_H^{(o)} = - \nabla_H p^{(o)} \ , \tag{3.13}$$

$$\nabla \cdot \underset{\sim}{u}_H^{(o)} = 0 \ , \tag{3.14}$$

$$\frac{\partial p^{(o)}}{\partial x_3} = - \rho^{(o)} \ , \tag{3.15}$$

$$\underset{\sim}{u}_H^{(o)} \cdot \nabla \rho^{(o)} - u_3^{(o)} \frac{d\bar{\rho}}{dx_3} = 0 \ , \tag{3.16}$$

and

$$\underset{\sim}{u}_H^{(o)} \cdot \nabla \psi^{(o)} = u_3^{(o)} \ . \tag{3.17}$$

Combining (3.16) and (3.17) gives

$$\underset{\sim}{u}_H^{(o)} \cdot \nabla \left[ \rho^{(o)} - \psi^{(o)} \frac{d\bar{\rho}}{dx_3} \right] = 0 \ .$$

Assuming $\rho^{(o)}$ and $\psi^{(o)}$ are zero in the free stream, then, since $\frac{d\bar{\rho}}{dx_3}$ is independent of $\underset{\sim}{x}_H$, one obtains

$$\rho^{(o)} = \psi^{(o)} \frac{d\bar{\rho}}{dx_3} \ ,$$

or with (3.15)

$$\psi^{(o)} = - \frac{\partial p^{(o)}}{\partial x_3} \Big/ \frac{d\bar{\rho}}{dx_3} \ . \tag{3.18}$$

Note that, from equations (3.13) and (3.14), the equations for $\underset{\sim}{u}_H^{(o)}$ and $p^{(o)}$ are those for an inviscid, two-dimensional flow in a horizontal plane. In particular, if the incoming (horizontal) flow is irrotational, then the entire horizontal flow field is irrotational. Thus, in this case the tools of the potential-flow theory can be employed to compute the flow. In a given horizontal plane, the resulting solution would be that of a two-dimensional flow about an obstacle defined by the contour of the terrain at the vertical level of that terrain. The vertical displacement can be computed from (3.18), where it is a result of the pressure difference in the flow between two

adjacent horizontal layers. A calculation of the vertical displacement can also be used to estimate the region of validity of the results.

Equations (3.13), (3.14) and (3.18) were programmed on the computer for flow past somewhat arbitrarily shaped terrain features. The free-stream flow was assumed irrotational, and standard numerical procedures for computing the two-dimensional potential flow past arbitrarily shaped bodies were used. Details of the numerics are presented in the appendix.

## SECTION IV

## DESCRIPTION OF THE EXPERIMENT

The experimental setup was basically the same as that discussed in Flow Research Report No. 57 (Liu and Lin, 1975), which describes Task I of this study. In addition to the idealized terrain model, which has been used for detailed studies in the past (see Flow Research Report No. 29) and is defined by

$$h_I(\hat{x}_1,\hat{x}_2) = 17.8 \left\{ \exp\left[ - .0008513(\hat{x}_1 - 61)^2 - .01197(\hat{x}_2 - 18.82)^2 \right] + \exp\left[ -.0008513(\hat{x}_1 - 61)^2 - .01197(\hat{x}_2 + 18.82)^2 \right] \right\} + 16 \left\{ \exp\left[ -.01171(\hat{x}_1 - 61)^2 - .002314\, \hat{x}_2^2 \right] \right\} , \tag{4.1}$$

we used a conically shaped model,

$$h_C(\hat{x}_1,\hat{x}_2) = \begin{cases} 30\left(1 - \frac{r}{15}\right) & r \leq 15 \\ 0 & r > 15 , \end{cases} \tag{4.2}$$

and a Gaussian-shaped model,

$$h_G(\hat{x}_1,\hat{x}_2) = 30 \exp\left[ - \left(\frac{r}{20}\right)^2 \right] . \tag{4.3}$$

Here, $r = \left(x_1^2 + x_2^2\right)^{1/2}$ and all distances are measured in centimeters.

The two latter (new) models were designed to be interchangeable with the idealized model. Neutrally buoyant dyes, each of a different color, were released through small stainless-steel tubes (.3 mm I.D.) at three levels upstream of the model. Three plumes spaced in the horizontal were released in each level. The plume trajectories were photographed, and then analyzed for later comparisons with analytical results. Figure 2 shows a typical side view of the streak-line patterns for flow past the Gaussian peak.

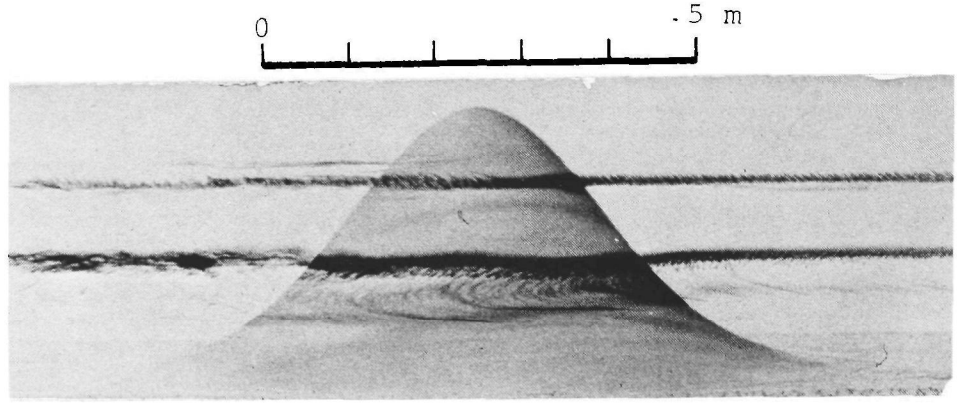


a. U = 1.5 cm/s, $F_h$ = .37

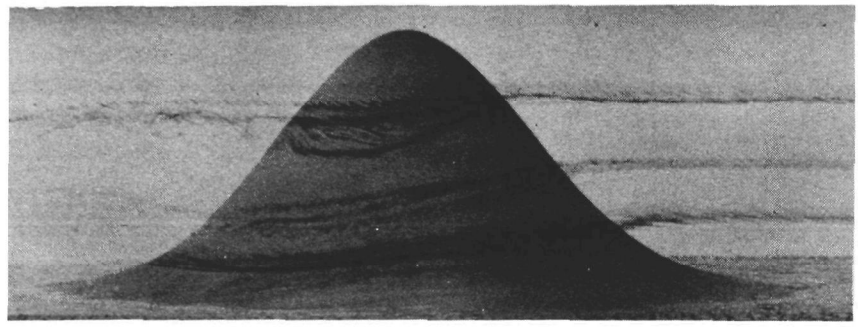

b. U = 4 cm/s, $F_h$ = .97

Fig. 2 The Flow Patterns Traced by Neutrally Buoyant Dye in the Vicinity of a Three-Dimensional Gaussian-Shaped Model. N = .135 Hz.

Note that in each horizontal plane, three streak lines were released. However, in the side view, the three are difficult to distinguish, especially in the lowest Froude number cases. This difficulty is somewhat compounded by the slight vertical spread of each streak line. However, in a given horizontal plane, the innermost streak line is displaced more than the others, so that its displacement is easily detectable in the photographs. Thus, when comparisons were made, we used the innermost streak line.

Other cases are presented in a 16 mm movie, which is a part of the Task I report. Table 1 presents the conditions for the runs, and table 2 shows appropriate upstream positioning of the dye release. In these tables, $F_h = \frac{2\pi U}{Nh} = 2\pi F$ is the defining Froude number.

The choice of the model conditions was based on the following criterion. The expansion can only remain valid as long as streamlines do not cross in the vertical. This crossing would occur, for example, if $\hat{\psi}_1 > \hat{\psi}_2 + \Delta\hat{x}_3$ (figure 3). Thus, $-\Delta\hat{x}_3 > \hat{\psi}_2 - \hat{\psi}_1$, or in the limit, as $\Delta\hat{x}_3 \to 0$,

$$-\frac{\partial\hat{\psi}}{\partial\hat{x}_3} \geq 1 \ .$$

When one considers both upward and downward displacements, this condition generalizes to

$$\left|\frac{\partial\hat{\psi}}{\partial\hat{x}_3}\right| \geq 1 \ .$$

Thus, in nondimensional terms, a necessary condition for the validity of the expansion is

$$F^2 \left|\frac{\partial\psi}{\partial x_3}\right| \leq 1 \ . \qquad (4.4)$$

We selected the various parameters in the experiments so that (4.4) was satisfied over a large portion of the vertical region of interest.

TABLE 1. EXPERIMENTAL PARAMETERS

| Run Number | Terrain Model | Stratification Profile | $N_c$ (cycle/sec) | U (cm/sec) | $F_h$ |
|---|---|---|---|---|---|
| IVa | Conical Model (eq. (4.2)) | 1-Layer, Constant N | .135 | 1.5 | .37 |
| IVb | Conical Model | 1-Layer, Constant N | .135 | 3.0 | .74 |
| IVc | Conical Model | 1-Layer, Constant N | .135 | 6.0 | 1.48 |
| Va | Gaussian Model (eq. (4.3)) | 1-Layer, Constant N | .138 | 1.5 | .36 |
| Vb | Gaussian Model | 1-Layer, Constant N | .138 | 3.0 | .72 |
| Vc | Gaussian Model | 1-Layer, Constant N | .138 | 4.0 | .97 |
| VIa | Idealized Terrain Model (eq. (4.1)) | 1-Layer, Constant N | .135 | 3.0 | 1.37* |
| VIb | Idealized Terrain Model | 1-Layer, Constant N | .135 | 6.0 | 2.72* |

*Froude No. Based on the Interior Ridge Height

TABLE 2. UPSTREAM POSITIONS OF DYE RELEASE

| Terrain Model | Vertical Level (cm) (Measured From Terrain Model Base) | Horizontal Position (cm) (Measured From Terrain Model Centerline, $\hat{x}_2 = 0$) |
|---|---|---|
| Conical Model (eq. 4.2)) | 14.0 | 1.0 |
| | 14.0 | 5.0 |
| | 14.0 | 13.0 |
| Gaussian Model (eq. (4.3)) | 7.6 | 3.3 |
| | 7.6 | 8.4 |
| | 7.6 | 19.0 |
| | 13.2 | 2.1 |
| | 13.2 | 6.8 |
| | 13.2 | 17.1 |
| $\hat{x}_2$ | 20.3 | 0.6 |
| | 20.3 | 7.0 |
| | 20.3 | 17.5 |
| Idealized Terrain Model (eq. (4.1)) | 11.5 | 1.0 |
| | 11.5 | 5.0 |
| | 11.5 | 12.0 |

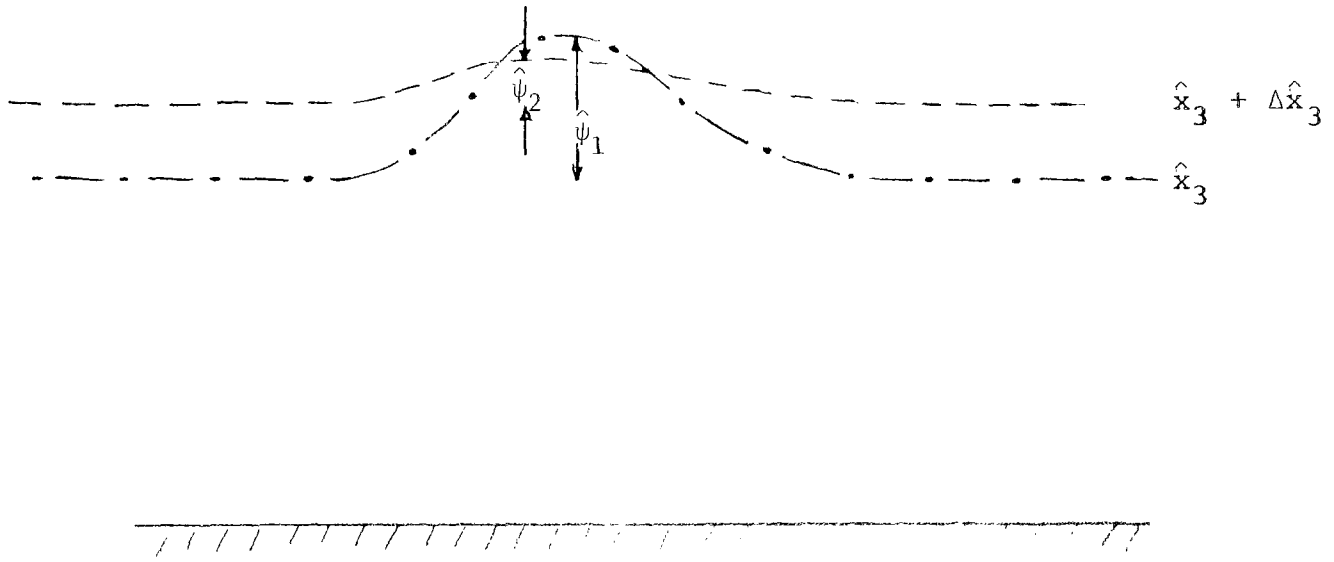


Figure 3. The Crossing of Streamlines in the Vertical.

## SECTION V

## COMPARISONS OF EXPERIMENTAL AND NUMERICAL RESULTS

As mentioned in the previous section, tables 1 and 2 give the experimental conditions. The general behavior of the streak lines can be seen by examination of figure 2b. In the middle horizontal plane, consider the inner streak line, which exhibits the largest vertical displacement. As a fluid element approaches the model, it slows down in a manner similar to an element in a two-dimensional flow about a cylinder. Simultaneously, the element experiences an upward pressure force, causing it to rise upward (see equation 3.18). As the element starts around the mountain, it accelerates, the vertical pressure force changes direction, and the element is displaced downward. The flow separates near the point of maximum lateral extension of the model. Past the midpoint of the mountain, the elements return to their equilibrium levels, and are entrained into the wake of the model. For the Froude number range in the experiments, the wake flow in the lee of the model appeared to consist of turbulent, quasi-horizontal eddies, whose vertical velocity fluctuations were rapidly decaying with downstream distance.

The incoming flow was slightly unsteady. We observed that the inner streak lines slowly oscillated from one side of the mountain to the other. This oscillation often produced an inner streak-line pattern, as sketched in figure 4. One possible explanation of this phenomenon is the following. For two-dimensional flow past a cylinder, turbulent vortex streets are observed in the Reynolds number range of about $60 \leq R \leq 5000$, where the Reynolds number R is $\frac{UD}{\nu}$, D is the diameter of the cylinder, and $\nu$ is the kinematic viscosity. For our case, R is typically

$$R \approx \frac{4 \text{ cm/sec} \times 10 \text{ cm}}{.01 \text{ cm}^2/\text{sec}} \approx 4000 ,$$

which is in this range. The vortex motion is accompanied by movement of the stagnation points, which in turn causes the incoming flow to oscillate slightly. For R in this range, the Strouhal number, defined by $S = \frac{nD}{U}$, where n is the vortex shedding frequency in radians/sec, is approximately .21. Thus,

$$\frac{n}{2\pi} \approx \frac{.21 \times 4 \text{ cm/sec}}{2\pi \times 10 \text{ cm}} \approx .014 \text{ cycles/sec} .$$

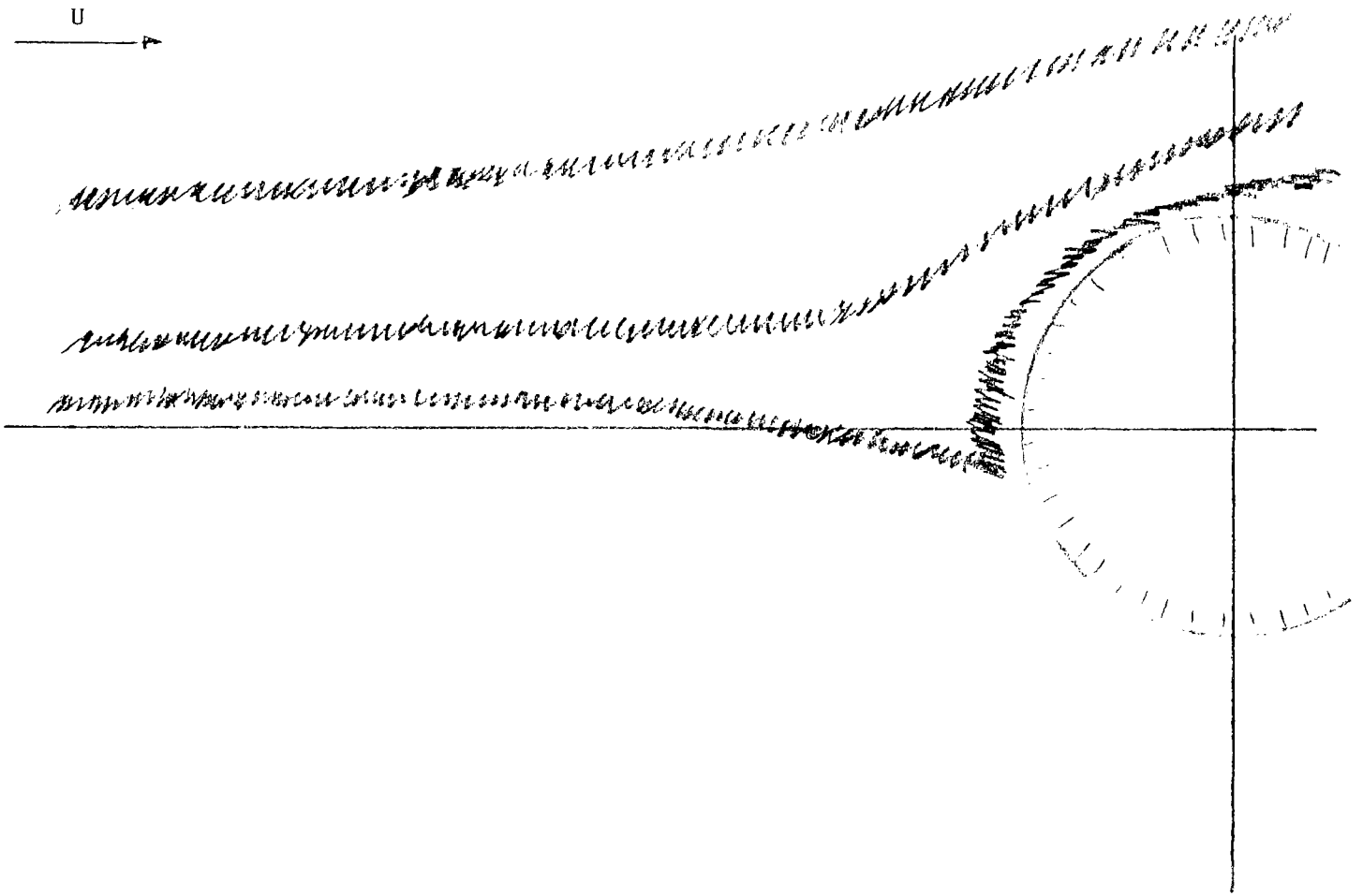




Figure 4. Sketch of the Instantaneous Streak-Line Pattern.

This value corresponds roughly to the frequency of the oscillations noted in the experiments.

Figure 5 shows streak lines in the horizontal plane, $\hat{x}_3$ = 13.2 cm (the middle plane) for the Gaussian model with F = .152 (or $F_h$ = .97, run number Vc). Also shown are the numerical predictions. In addition, the contour of the model at the free-stream level of the plumes is displayed. Note that the numerical calculation tends to underpredict streak-line displacement. This discrepancy is probably the result of mainly two effects. The first is the displacement effect of the boundary layer, which is not taken into account in the inviscid numerical model. The second and more important effect is the displacement effect of the separated wake. These two effects together produce an "apparent" body, as sketched in figure 6a.

Note that for a two-dimensional flow past a circular cylinder, if the Reynolds number is subcritical (i.e., below approximately $3 \times 10^5$), the boundary layer is laminar, and it separates at about 80° from the front stagnation point (Schlichtling, 1960). Since the Reynolds numbers for the experiments were an order of magnitude less than the critical value, it is reasonable to assume that the boundary layer was laminar and separated before the point of maximum lateral extension of the body. For two-dimensional flow past a circular cylinder, if the Reynolds number is supercritical, the boundary layer is turbulent, and separation probably occurs just past the point where the cross section starts to converge. Thus, in the full-scale case, where Reynolds numbers will usually be several orders of magnitude larger than the critical value, separation is likely to occur just past the point of maximum lateral extent.

When viscous terms are added to the scaling arguments presented in section 3, one finds that the lowest order solution is no longer two-dimensional. Thus, the conclusions drawn above could be modified somewhat because of the three-dimensional nature of the boundary layer.

The displacement effect of the separated wake was crudely modeled by extending the body, as shown in figure 6b. Figure 5 also shows the results of a calculation using this body shape instead of the circular shape. The modification of the streak lines, especially the outermost ones, is noticeable. However, from the discussion above, the model suggested in figure 6b is probably more adequate for the full-scale case than the laboratory case. Also, the effect of the boundary layer may have to be taken into account to obtain close agreement between the numerical and experimental results.

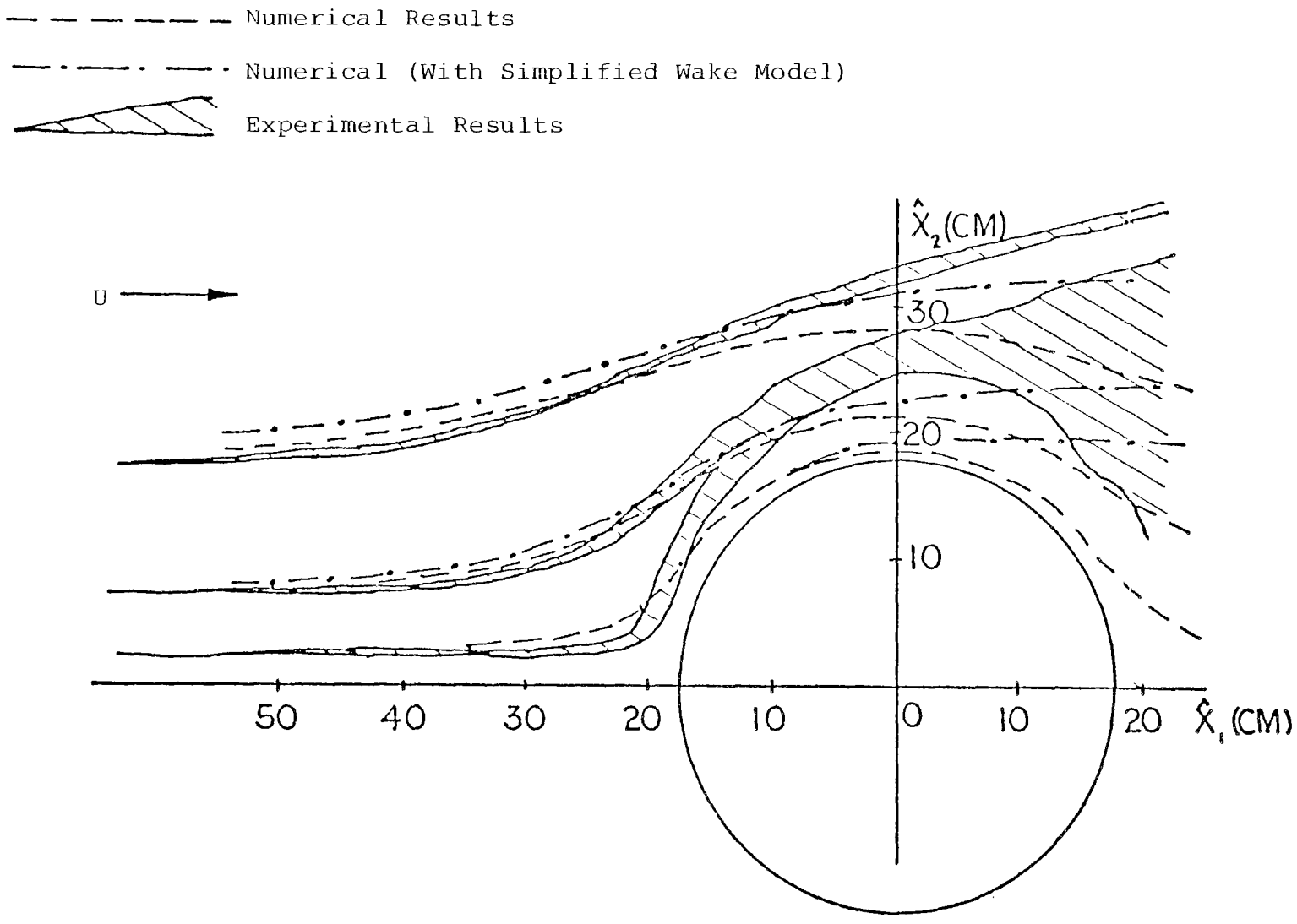


Figure 5. Comparison of Experimental & Numerically Computed Streak Lines in the Horizontal Plane Defined by $\hat{x}_3$ = 14 cm for Case Vc (Gaussian Model $F_h$ = .97).

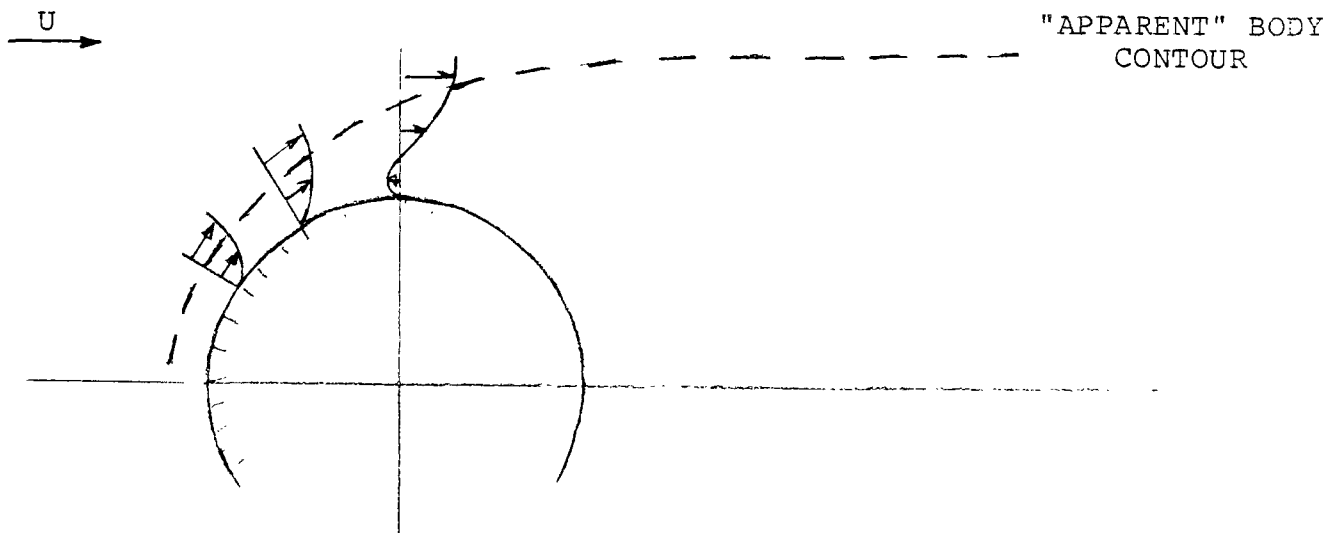


Figure 6a. Apparent Body Shape.

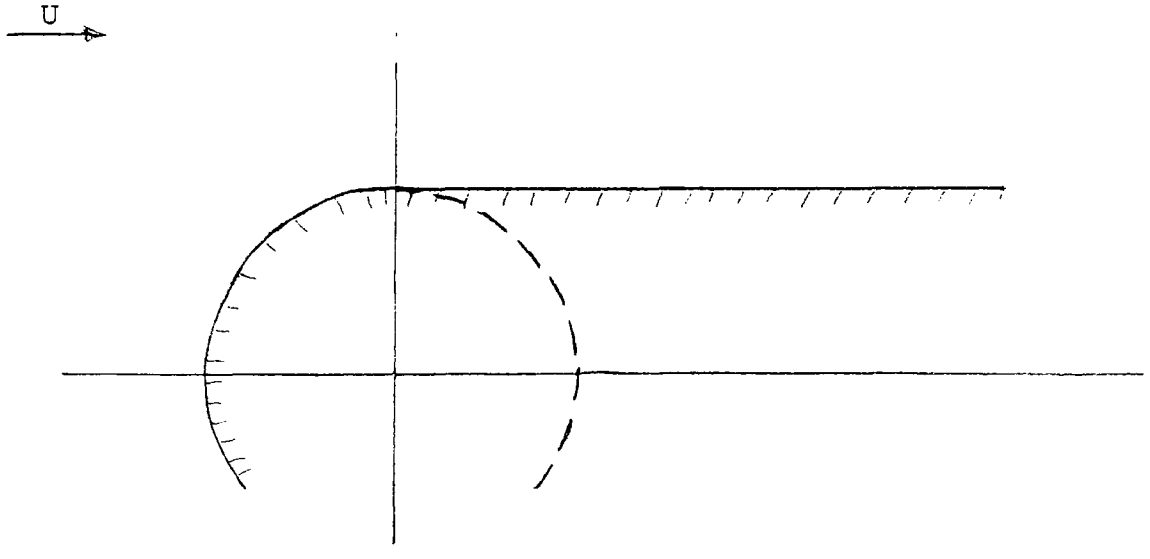


Figure 6b. Model for the Separated Wake.

The width of the tank is approximately 120 cm, so it is possible that the sidewalls influence the flow field near the models. Sidewalls were not included in the numerical models. However, the horizontal displacement of the streamline whose free-stream position is at the sidewalls was computed. For the Gaussian and conical models, the displacement of this streamline was negligible for the cases computed. Thus, for these cases, we can assume that the effect of sidewalls is unimportant.

Figure 7 shows a similar comparison for the conical model, in the middle horizontal plane ($\hat{x}_3$ = 14 cm), for F = .059 (or $F_h$ = .37, run number IVa). The results and interpretation are similar to that for the previous case. Note the multiple lines which describe the plume trajectories. For a particular dye release, the different lines come from photographs taken of the streak line at different times. The discrepancies in the experimental results are probably a result of the unsteadiness caused by the vortex shedding discussed above.

Figure 8 shows the experimentally determined vertical displacement for the conical model, run number IVa. Note for this case that the streak-line displacement was very slight--less than approximately .5 cm. The maximum displacement computed numerically was about .5 cm, in approximate agreement with experiment. The very small vertical displacement of the streak lines supports the original scaling assumptions for this case.

Figure 9 shows similar experimental plots for the conical peak at F = .109 (or $F_h$ = .74, run number IVb). Vertical displacements are much more noticeable in this case. This increase in displacement is expected, since it has been established (equation (3.5d)) that vertical displacement scales approximately as the square of the Froude number. Also shown in this plot is the numerical prediction for the innermost plume in the middle level. The numerical calculation predicts a very slight rise in the plume as it approaches the mountain, which is also discernible in the experiments. The distance that the plume drops is also predicted fairly well. However, the asymmetry of the experimental results is missed entirely. This discrepancy is again probably attributable to the neglect of the boundary layer and wake effects.

Figure 10 shows similar experimental plots for the Gaussian model at F = .152 (or $F_h$ = .97, run number Vc). Also shown are the numerical predictions for the innermost plume for each of the three levels. The agreement and explanation of the results are very similar to the previous case.

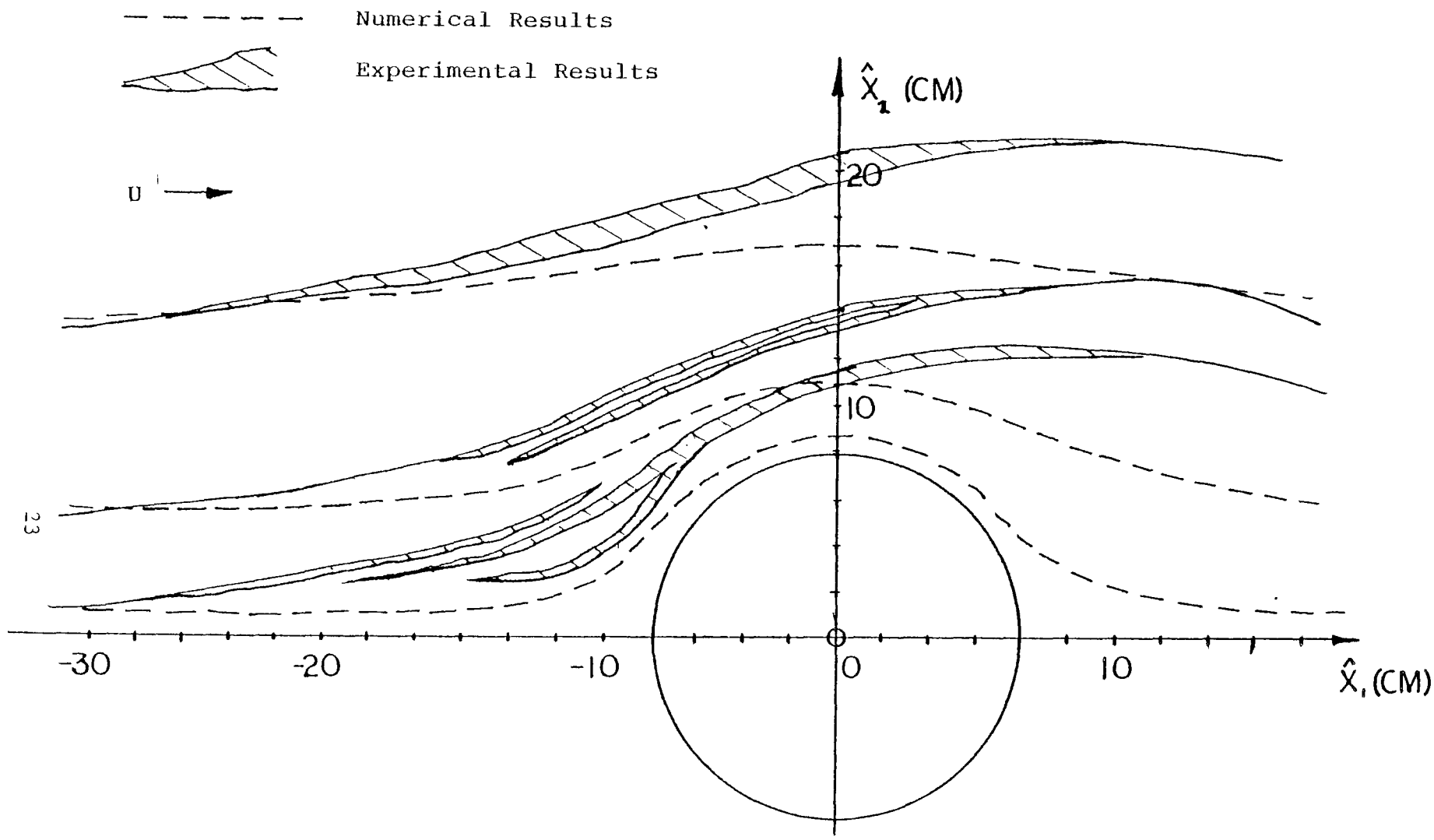


Figure 7. Comparison of Experimental & Numerically Computed Streak Lines on the Horizontal Plane Defined by $\hat{x}_3$ = 14 cm for Case IVa (Conical Model, $F_h$ = .37)

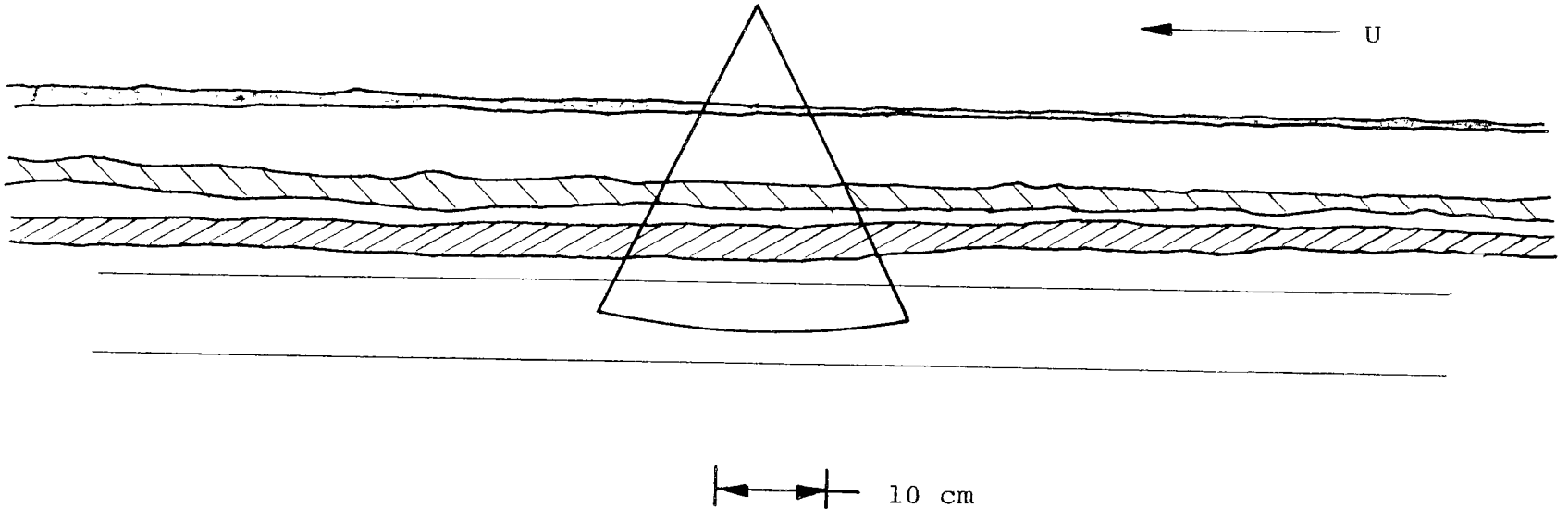


Figure 8. Experimental Results For Vertical Displacement For Case IVa (Conical Model $F_h$ = .37)

Solid Lines = Experimental Results

Dotted Line = Numerical Results

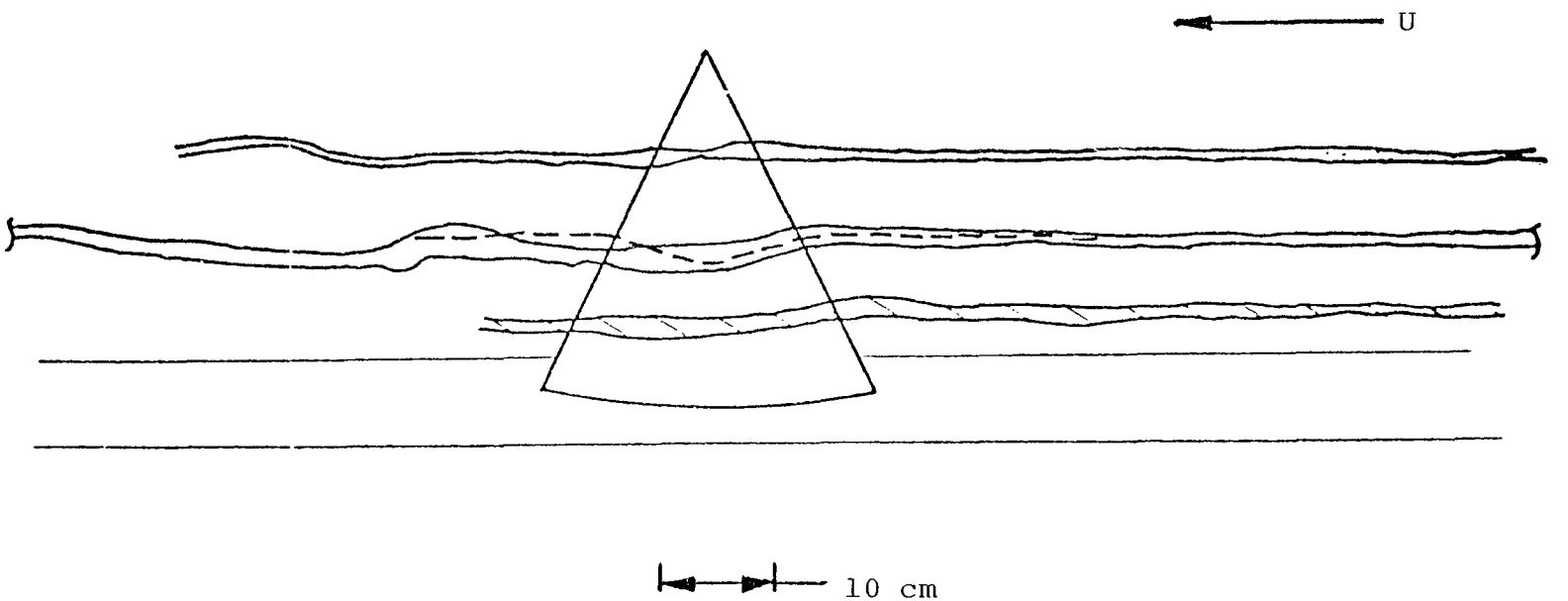


Figure 9. Comparison of Experimental & Numerically Computed Results For Vertical Displacement For Case IVb (Conical Model $F_h$ = .74).

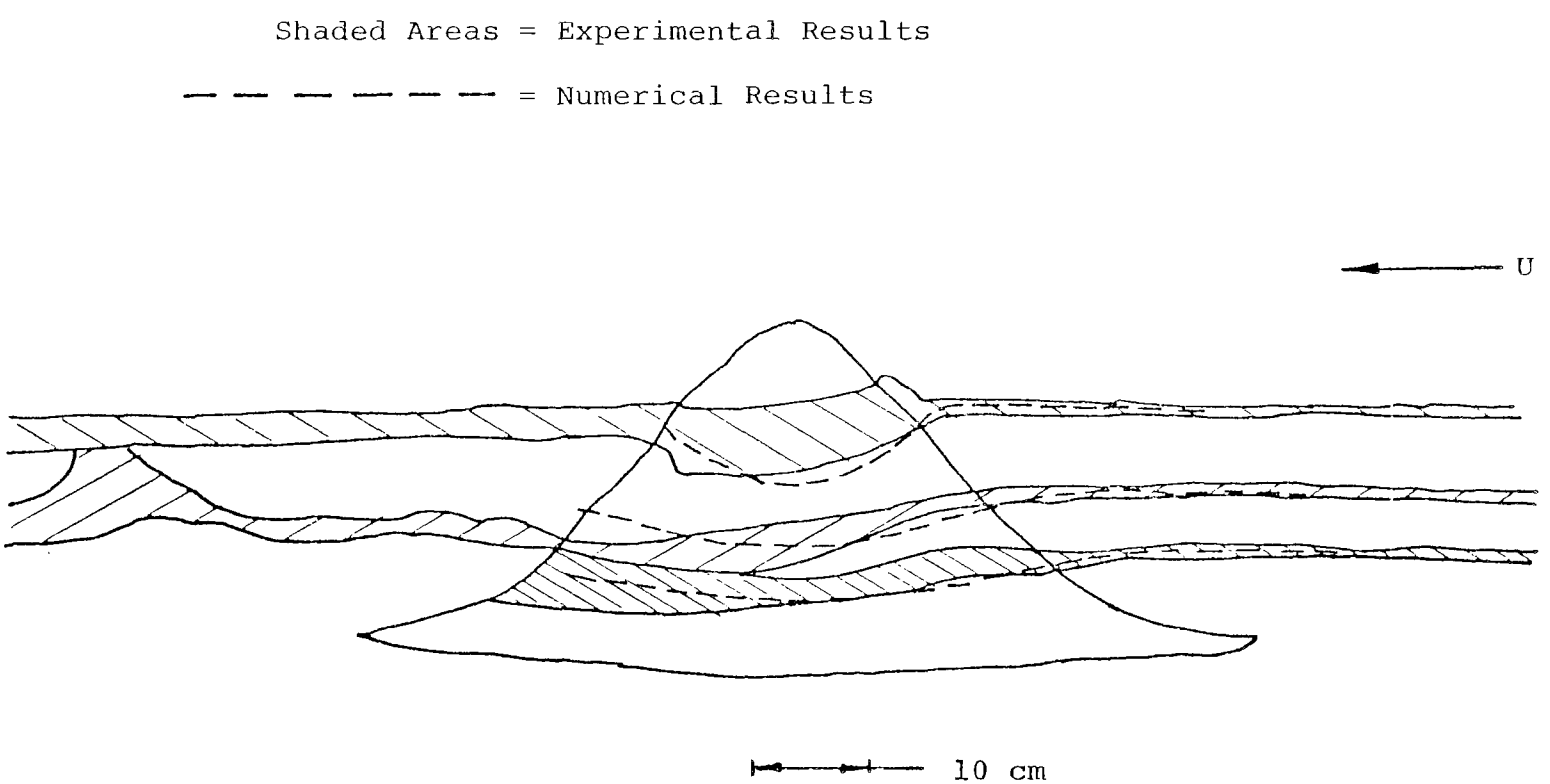


Figure 10. Comparison of Experimental and Numerically Computed Results for Vertical Displacement for Case Vc (Gaussian Model, $F_h$ = .97).

Finally, figure 11 shows comparisons of experimentally observed and numerically computed streak lines for the idealized terrain case, with $F_h = .137$ The dye was released at approximately $\hat{x}_3 = 11.5$ cm. Note that the calculation included separation in the wake, in the manner discussed above. Comparisons for this case are much better than for the previous cases because the crude wake modeling for the potential flow calculation closely matched the real flow. In the calculations for the previous cases, the assumption that the separation stream line is straight and parallel to the upstream flow direction was not supported by the experimental results which indicate a diverging wake region.

An examination of the side view shows sizeable vertical displacement as the stream lines traverse the ridge. This is accompanied by some motion towards the ridge, resulting in the inner plume appearing to cut through the terrain in the top view. As the fluid comes over the ridge, it tends to fall below its ambient level, thus forcing the fluid laterally away from the ridge, and producing the slight bulge seen in the figure above the ridge. This bulge may also be attributable to a boundary layer separation bubble. According to the potential flow calculation, the boundary layer is subjected to an adverse pressure gradient near the most upstream point on the model. Therefore, separation of the laminar boundary layer is likely.

Finally, calculations of the streamline at the location of the tank sidewall show that its lateral displacement is significant. Thus, sidewall effects, which were neglected in the calculation, could be of some importance in this case.

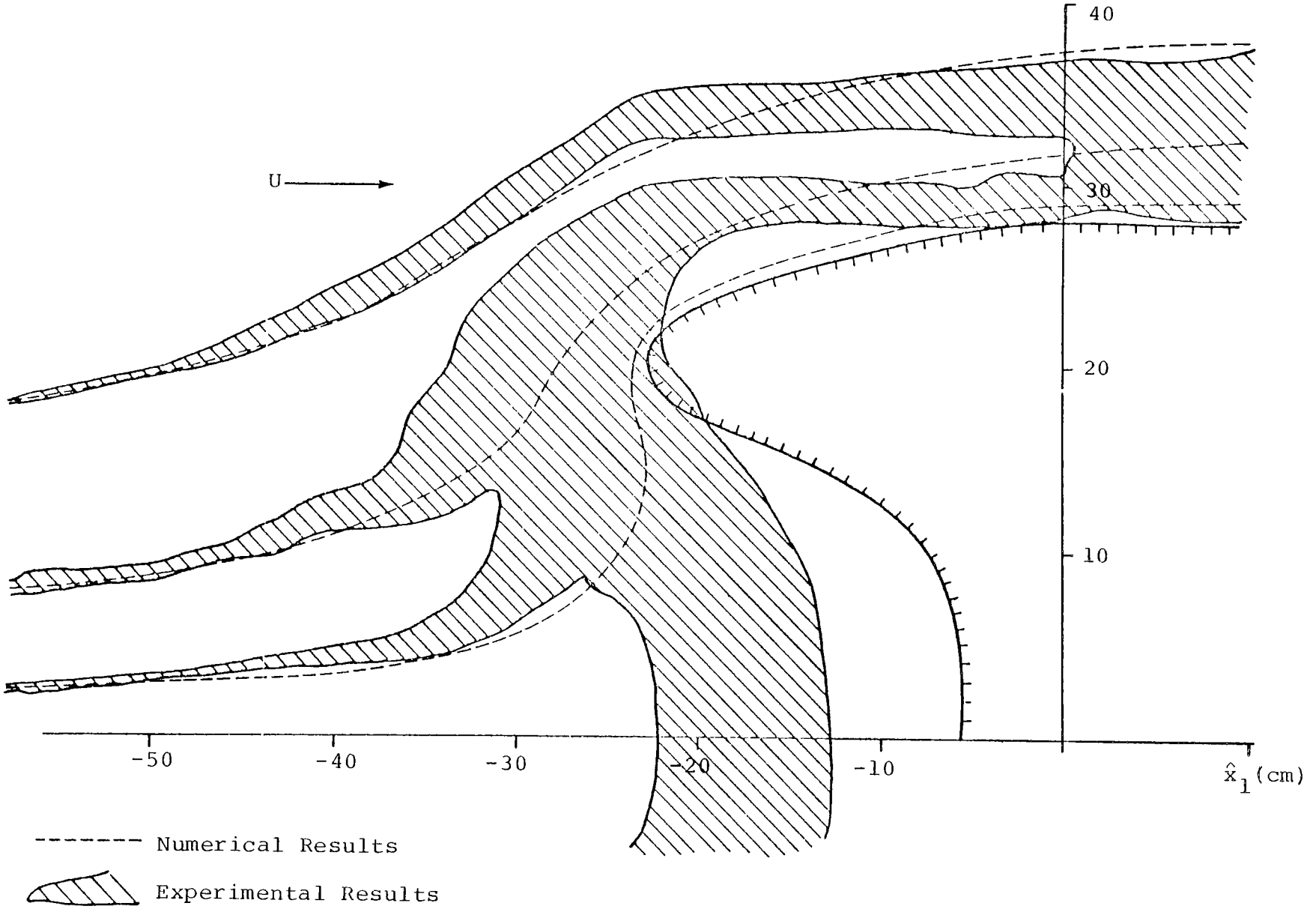


Figure 11. Comparison of Experimental & Numerically Computed Streak Lines in the Horizontal Plane Defined by $\hat{x}_3$ = 11.5 cm (Idealized Terrain Model, $F_h$ = 1.37).

## REFERENCES


Drazin, P. G. (1961), "On the Steady Flow of a Fluid of Variable Density Past an Obstacle," Tellus 13, 239-251.

Lilly, D. K. (1973), "Calculation of Stably Stratified Flow Around Complex Terrain," Flow Research Note No. 40.

Lin, J. T., Liu, H. T. and Pao, Y. H. (1974), "Laboratory Simulation of Plume Dispersion in Stably Stratified Flows Over Complex Terrain," Flow Research Report No. 29.

Liu, H. T. and Lin, J. T. (1975), "Plume Dispersion in Stably Stratified Flows Over Complex Terrain: Phase II," Flow Research Report No. 57.

Phillips, O. M. (1966), The Dynamics of the Upper Ocean, Cambridge University Press.

Schlichting, H. (1960), Boundary Layer Theory, McGraw Hill.

## APPENDIX: NUMERICAL METHODS

The basic numerical problem involves computing the two-dimensional potential flow about an arbitrarily shaped body. The streamlines are found using the stream function, and the vertical displacement is determined by computing the pressure field at two adjacent levels, and then using a simple differencing scheme (see equation (3.18)).

The two-dimensional potential flow about a closed contour is constructed by combining a uniform flow with the velocity field of a vorticity sheet located on the contour. The uniform flow is chosen to give the desired flow at infinity, and the distribution of the vorticity strength is found such that the prescribed boundary condition on the contour is satisfied. For this work the boundary condition is that the flow be tangent to the contour (i.e., zero velocity component normal to the contour).

The governing integral equation expressing the boundary condition is solved numerically for the vorticity distribution by approximating the contour with an inscribed polygon and by assuming that the vorticity varies linearly with the arc length along each segment of the polygon. With no discontinuities in strength at the polygon corner points, this approximating vorticity distribution is defined by the corner-point values. Enforcing the boundary condition at the midpoints of the segments gives a set of algebraic equations in terms of the unknown vorticity corner-point values.

An additional relation is needed to obtain a unique solution to these equations. For this work the circulation about the contour was required to vanish. This requirement provides an additional algebraic equation in the unknown vorticity corner-point values.

After obtaining the approximating vorticity sheet from the numerical solution of the governing integral equation, we construct the velocity field and the stream function field associated with the vorticity sheet and add them to the free-stream contributions to obtain the desired results.

The pressure field is obtained from the velocity field using the incompressible Bernoulli relation.

TECHNICAL REPORT DATA
*(Please read Instructions on the reverse before completing)*

| 1. REPORT NO. | 2. | 3. RECIPIENT'S ACCESSION NO. |
|---|---|---|
| EPA-600/4-76-021 | | |

| 4. TITLE AND SUBTITLE | 5. REPORT DATE |
|---|---|
| A NUMERICAL AND EXPERIMENTAL STUDY OF STABLY STRATIFIED FLOW AROUND COMPLEX TERRAIN | May 1976 |
| | 6. PERFORMING ORGANIZATION CODE |
| 7. AUTHOR(S) | 8. PERFORMING ORGANIZATION REPORT NO. |
| J. J. Riley, H. T. Liu and E. W. Geller | Flow Research Report No. 58 |
| 9. PERFORMING ORGANIZATION NAME AND ADDRESS<br>Flow Research, Inc.<br>1819 South Central Avenue<br>Kent, Washington 98031 | 10. PROGRAM ELEMENT NO.<br>1AA009 |
| | 11. CONTRACT/GRANT NO.<br>68-02-1293 |
| 12. SPONSORING AGENCY NAME AND ADDRESS<br>Environmental Sciences Research Laboratory<br>Office of Research and Development<br>U. S. Environmental Protection Agency<br>Research Triangle Park, NC 27711 | 13. TYPE OF REPORT AND PERIOD COVERED<br>Final Report, 5/74-3/75 |
| | 14. SPONSORING AGENCY CODE<br>EPA - ORD |
| 15. SUPPLEMENTARY NOTES | |

16. ABSTRACT

A computer program was developed to compute three-dimensional stratified flow around complex terrain for the case of very strong stratification (small internal Froude number). Laboratory experiments were performed for strongly stratified flow past three different terrain models for comparison. The computed results are in fair agreement with the experiments for the cases of two simpler terrain models. The discrepancies are probably attributable to the separated wake in the lee of the models. The agreement was not as good for the case of the more complex terrain. Possible sources of error are discussed in some detail.

17. KEY WORDS AND DOCUMENT ANALYSIS

| a. DESCRIPTORS | b. IDENTIFIERS/OPEN ENDED TERMS | c. COSATI Field/Group |
|---|---|---|
| *Mathematical models | | 12A |
| *Plumes | | 21B |
| *Stratification | | 14G |
| *Terrain | | 08F |
| *Air pollution | | 13B |

| 18. DISTRIBUTION STATEMENT | 19. SECURITY CLASS *(This Report)* | 21. NO. OF PAGES |
|---|---|---|
| RELEASE TO PUBLIC | UNCLASSIFIED | 41 |
| | 20. SECURITY CLASS *(This page)* | 22. PRICE |
| | UNCLASSIFIED | |

EPA Form 2220-1 (9-73)